ORIGINAL ARTICLE

Microwave-assisted rapid synthesis of Co_3O_4 nanorods from $CoC_2O_4.2H_2O$ nanorods and its application in photocatalytic degradation of methylene blue under visible light irradiation

Sadigheh Bazgir; Saeed Farhadi*

Department of Chemistry, Lorestan University, Khoramabad, Iran

Abstract
In this work, Co_3O_4 nanorods were successfully prepared by microwave-assisted solid state decomposition of rod-like $CoC_2O_4.2H_2O$ precursor within a very short reaction time (6 min) without the use of a solvent/surfactant and complicated equipment. The as-obtained Co_3O_4 nanorods were fully characterized by X-ray diffraction (XRD), Fourier transform infrared spectroscopy (FT-IR), Raman spectroscopy, scanning electron microscopy (SEM), transmission electron microscopy (TEM), ultraviolet–visible spectroscopy (UV–Vis), energy-dispersive X-ray spectroscopy (EDX), and magnetic measurements. TEM and SEM images showed that the Co_3O_4 nanorods have a length of 1-3 μm and diameter of 40-80 nm. FT-IR, XRD, EDX and selected-area electron diffraction demonstrated that the nanorods are composed of pure cubic phase Co_3O_4. Magnetic measurements at room temperature suggested the existence of a weak ferromagnetic behavior. The optical spectrum indicated two direct band gaps at 2.20 and 3.60 eV with a blue shift compared with the bulk sample. The photocatalytic activity of Co_3O_4 nanorods was investigated for the degradation of methylene blue (MB) as a model of dye pollutants in the presence of H_2O_2 as a green oxidant. The Co_3O_4 nanorods showed high efficiency for the degradation of MB dye by using H_2O_2 under visible light irradiation. Trapping experiments indicated that hydroxyl (•OH) radicals were the main reactive species for dye degradation in the present photocatalytic system. In addition, the possible photodegradation mechanism was also proposed based on the trapping experiment results.

Keywords: Co_3O_4 *nanorods; Methylene blue dye; Microwave irradiation; Photocatalytic degradation; Transition metal oxides.*

INTERODUCTION

In recent years, nanostructured transition metal oxides with special shapes and morphologies have received much attention owing to their strong physical properties for optical, electrical, and magnetic applications, which are very important for the development and realization of photoelectronic devices with high performance [1-3]. It is well known that the structure, size, and morphology significantly influence the properties and application of the materials. Controlling the morphology of inorganic nanomaterials through appropriate synthetic methods plays a key role in obtaining nanomaterials with novel properties.

* Corresponding Author Email: *sfarhadi1348@yahoo.com*

Among various transition metal oxides, spinel-type cobalt oxide (Co_3O_4), either in bulk or nanocrystalline form is known as a promising p-type semiconducting material that exhibits various potential applications in low temperature CO oxidation, oxidation of volatile organic compounds (VOCs) and ammonia, N_2O and H_2O_2 decomposition, anode materials in Li-ion rechargeable batteries, gas sensing, and magnetic materials [4-13]. Owing to the influence of particle size and morphology on the properties of materials, research interesting has been focused on controlling preparation of Co_3O_4 particles with different sizes and morphologies because the

S. Bazgir and S. Farhadi

morphologies and sizes of nanomaterial have a significant effect on improving their performances. So far, well-defined Co_3O_4 nanostructures with various morphologies including tube, cube, wire, wall, sphere, sheet, nanocomposite film and flower-like nanostructures have been synthesized successfully by various strategies, such as thermal decomposition of cobalt precursors, chemical vapor deposition, pulsed laser deposition, combustion method, biotemplating technique, sonochemical method, co-precipitation method, hydro/slovothermal method, and traditional sol-gel method etc [14-41]. However, most of these methods have some drawbacks including long-time reaction, usage of toxic and expensive solvents, complicated synthetic steps, low production yields, high temperature preparation and requirement of external additives during the reaction which limits the purity of the products. In addition, another limitation of the traditional methods is the necessity of post reaction thermal treatment of the materials to increase the crystallinity, which is easy to result in particle aggregation and uncontrolled crystal growth. Hence, it is necessary to develop a simple, inexpensive, and environmental-friendly approach to the synthesis of Co_3O_4 structures at a relatively low temperature.

From a practical and environmental viewpoint, it is of importance to develop a simple, rapid and low-cost synthesis route to synthesize inorganic nanomaterials. Therefore, it still has enough room for exploiting a facile, convenient and additive free method to synthesize Co_3O_4 nanostructure with a special shape. Microwave irradiation (MWI)-assisted preparation has emerged as an appropriate and efficient route for the preparation of metal oxides nanostructures due to its simplicity, low-cost and multiplicate morphologies of products [42]. In the last three decades, numerous applications of MWI to prepare nanostructured materials have been reported [43]. Compared to conventional methods, the MWI-based method is faster, cleaner, and more economical. Further, it gives products with smaller particle size, narrow size distribution, and high purity.

Within the last decades, the photocatalytic degradation of organic pollutants in the presence of semiconductors has attracted increasing interest because it is a promising, environmental, and cost-effective technology for the treatment of contaminated groundwater and wastewater

[44-47]. To better utilize visible light accounting for about 43% of solar energy, great efforts have been made to exploit visible-light-sensitive photocatalysts. Titanium dioxide (TiO_2) is the most widely studied and promising photocatalyst owing to its low cost, high chemical and photochemical stability [48]. Nevertheless, the photocatalytic efficiency of TiO_2 is limited under the visible light because of its wide band gap and high electron-hole recombination rate. Different surface modification methods have been carried out to shift the absorption edge of TiO_2 into the visible region [49-54]. Among them, fabrication of semiconductor metal oxides with special shape and morphology is an effective method to improve the stability, photocatalytic efficiency and prevent the aggregation of nanoparticles [55-58]. Although, enormous efforts have been devoted to preparation and potential applications of Co_3O_4 nanostructures in catalysts, gas sensors, and lithium-ion batteries, but there are only a few reports on their photocatalytic properties of Co_3O_4 nanostructures [59-62].

On the basis of the above discussions, in this work, we present a facile and simple method to fabricate rod-like Co_3O_4 nanostructure with the diameter of about 40-80 nm via MWI-assisted solid state decomposition of the rod-like $CoC_2O_4 \cdot 2H_2O$ precursor within 6 min. The method is fast, mild, energy-efficient, and environmentally friendly route to produce Co_3O_4 nanorods in only one step. The structure, morphology, and optical properties of the obtained nanomaterial were characterized in detail. The photocatalytic activity of the Co_3O_4 nanomaterial for the degradation of MB under visible light irradiation was also investigated. In addition, the possible photodegradation mechanism was proposed based on the trapping experiment results.

EXPERIMENTAL
Preparation of Co_3O_4 nanorods

Firstly, the $CoC_2O_4 \cdot 2H_2O$ precursor was prepared by adding an aqueous solution of $K_2C_2O_4$ to an aqueous solution of $Co(NO_3) \cdot 6H_2O$ under continuous stirring, according to the method described in the literature [63]. The resulting pinkish precipitate was separated and washed with water, ethanol, and diethyl ether and dried at 70°C in an oven. To prepare Co_3O_4 nanorods, the $CoC_2O_4 \cdot 2H_2O$ precursor (1 g) was taken in a small porcelain crucible and placed in the middle

S. Bazgir and S. Farhadi

of another larger porcelain crucible filled with CuO powder as a secondary MWI absorber. This assembly was then exposed to MWI in a microwave oven (LG–intellowave, 900 W, 2.45 GHz) operated at the power level of 360 W (40%) in the air. At the same time, decomposition of the precursor powder was initiated and completed after an irradiation time of 6 min. The decomposition product was cooled to room temperature and collected for characterization.

Characterization techniques

Infrared spectra were recorded on a Schimadzu system FT–IR 160 spectrophotometer using KBr pellets. The composition and phase purity of the as-prepared product was determined by a Rigaku D/max C III X-ray diffractometer using Ni-filtered Cu Kα radiation (λ = 1.5406 Å). XRD patterns were recorded in the 2θ range of 10°–80° with a scanning step of 0.02°. Raman spectrum measurement was carried out on a Spex 1403 Raman spectrometer. The optical absorption spectrum was recorded at room temperature on a Shimadzu 1650 PC UV–Vis spectrophotometer. The Co_3O_4 sample for UV-Vis studies was well dispersed in distilled water by sonicating for 25 min to form a homogeneous suspension. The size and morphology of the as-prepared product were observed by a transmission electron microscope (TEM, Philips CM10) and a scanning electron microscope (SEM, Philips XL-30SEM) equipped with an energy dispersive X-ray spectroscopy. For the TEM measurement, the powders were ultrasonicated in ethanol and a drop of the suspension was dried on a carbon-coated micro grid. Magnetic measurements were carried out at room temperature by using a vibrating sample magnetometer (VSM, Meghnatis Kavir Kashan Co., Kashan, Iran).

Photocatalytic tests

The visible light photocatalytic activity of the Co_3O_4 nanorods was evaluated by the degradation of methylene blue (MB). A 300 W Xe lamp with a cut-off filter was used as the light source to provide visible light irradiation (λ ≥ 420 nm). In a typical photocatalytic reaction, 30 mg of the Co_3O_4 nanorods and 1 mL H_2O_2 (30 %) were added to 50 ml of 25 mg/L MB aqueous solution. Prior to the light illumination, the mixture was stirred with a magnetic stirrer in the dark for 30 min to establish adsorption-desorption equilibrium between the solution and catalyst. At a given

time interval, 4 mL suspension was sampled and centrifuged to remove the photocatalyst particles. The degradation process and the concentration changes of MB dye were monitored by measuring the characteristic absorption of MB at 663 nm on a UV-vis spectrophotometer. All the aqueous samples were at natural pH (*ca.* 6.5) and all experiments were carried out at room temperature. The effect of the catalyst dosage (10, 20, and 30 mg in 50 mL dye solutions) was studied on the photocatalytic degradation of MB.
To test the recyclability, after the dye had been completely degraded, the Co_3O_4 nanorods was separated and washed with deionized water three times before the next run.

Active species trapping experiments

In order to examine the active species during the photocatalytic process, the free radical trapping experiments were performed. Disodium ethylenediamine tetra acetate (Na_2EDTA; 5 mmol L^{-1}), isopropyl alcohol (IPA; 5 mmol L^{-1}), and $AgNO_3$ (Ag^+; 5 mmol L^{-1}) were used as the scavengers of hole (*h*⁺), hydroxyl radical (•OH) and electron (*e*⁻), respectively. The test methods were similar to the above photocatalytic experiments.

RESULTS AND DISCUSSION
Characterization of Co_3O_4 nanorods

The FT-IR spectra of $CoC_2O_4.2H_2O$ complex and its final decomposition product under MWI are shown in Fig. 1. For the starting complex in Fig. 1(a), the characteristic stretching bands of $C_2O_4^{2-}$ groups are observed at about 1650,1350, 1315 and 800 cm^{-1} [64]. The broad band at about 3400 cm^{-1} is assigned to the water of hydration. As shown in the Fig. 1(b), all bands of the complex disappeared and only two characteristic bands of the spinel-type Co_3O_4 structure at 661.54 and 566.10 cm^{-1} are observed for the sample decomposed under MWI. The former band is characteristic of the Co^{3+}–O vibration in an octahedral site, and the later band is attributable to the Co^{2+}–O vibration in a tetrahedral site of the spinel-type Co_3O_4 lattice [65-66].

Fig. 2 shows the XRD pattern of the $CoC_2O_4.2H_2O$ complex and its final decomposition product under MWI for 6 min. All the diffraction peaks in Fig. 2(a) are in good agreement with JCPDS file of the $CoC_2O_4.2H_2O$ complex (JCPDS No. 25-0250). As we can clearly see in Fig. 2(b), after MWI all peaks related to the complex were removed and new

diffraction pattern appeared. The pattern reveals diffraction peaks with 2θ values at 19.50°, 31.37°, 37.02°, 39.10°, 44.97°, 55.84°, 59.58°, 65.46° and 77.62° that are assigned to the crystal planes of (111), (220), (311), (222), (400), (422), (511), (440) and (533) of crystalline Co_3O_4 phase, respectively, consistent with the literature values (JCPDS Card No. 76-1802). No peaks due to the impurities were detected, indicating that the Co_3O_4 was rather pure. This result confirms that the complex was decomposed completely into the Co_3O_4 phase in consistent with the FT-IR data. Using the Scherrer equation [67], the average sizes of the nanoparticles composing the nanorods were roughly estimated to be ~ 25 nm. According to the above results, the formation of Co_3O_4 from the $CoC_2O_4.2H_2O$ complex under MWI can be written as follows:

$$3CoC_2O_4.2H_2O \text{ (s)} + 2O_2(g) + MWI \rightarrow Co_3O_4(s)$$
nanorods + $6CO_2(g)$ + $6H_2O(g)$
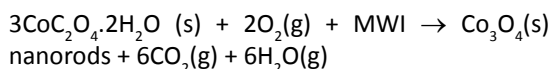
The morphology of $CoC_2O_4.2H_2O$ precursor and its decomposition product under MWI were investigated by SEM. Fig. 3(a) and (b) show the SEM micrographs of the $CoC_2O_4.2H_2O$ precursor at two different scales. It is obvious that the starting precursor was made of large and smooth nanorods with different sizes. The precursor displays rod-like

morphology with an average diameter of 80 nm and length of several micromeers. Fig. 3(c) and (d) show the morphology of the product obtained under MWI for 6 min. The SEM micrographs of the product powder clearly show that the shape and morphology of the product are quite similar to those of the precursor complex. As shown in the SEM images, the obtained Co_3O_4 product has rod-like shapes with weak agglomeration. It can be seen that most of the Co_3O_4 nanorods are in the size with lengths of 1–3 μm. It can be seen that the nanorods are straight and uniform along its whole length. Further, SEM image with higher magnification (Fig. 3(d)) shows that the nanorods are composed of spherical Co_3O_4 nanoparticles with a diameter ranging from 20 to 30 nm, which is consistent with the above-calculated value by the Scherrer equation from the XRD data**.**

The size and structure of Co_3O_4 nanorods have been investigated in detail by using TEM and selected-area electron diffraction (SAED) as shown in Fig. 4. The TEM samples were prepared with the dispersion of powder in ethanol by ultrasonic vibration. Fig. 4(a) and (b) show TEM images of individual and single Co_3O_4 nanorods with the diameter in the range of 40 to 80 nm and lengths up to 3μm. Further, TEM image with higher magnification in Fig. 4(c) shows the nanorods are
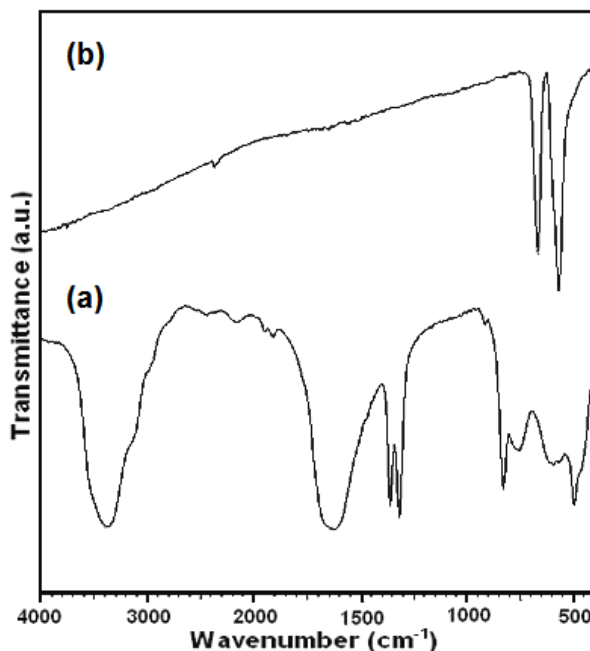

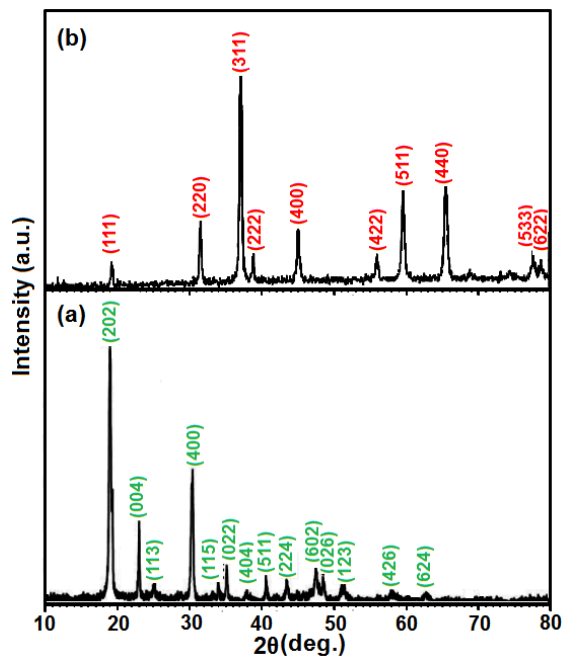Fig. 1: FT-IR spectra of (a) the $CoC_2O_4.2H_2O$ complex and (b) its decomposition product under MWI.

Fig. 2: XRD patterns of (a) the $CoC_2O_4.2H_2O$ complex and (b) its decomposition product under MWI.
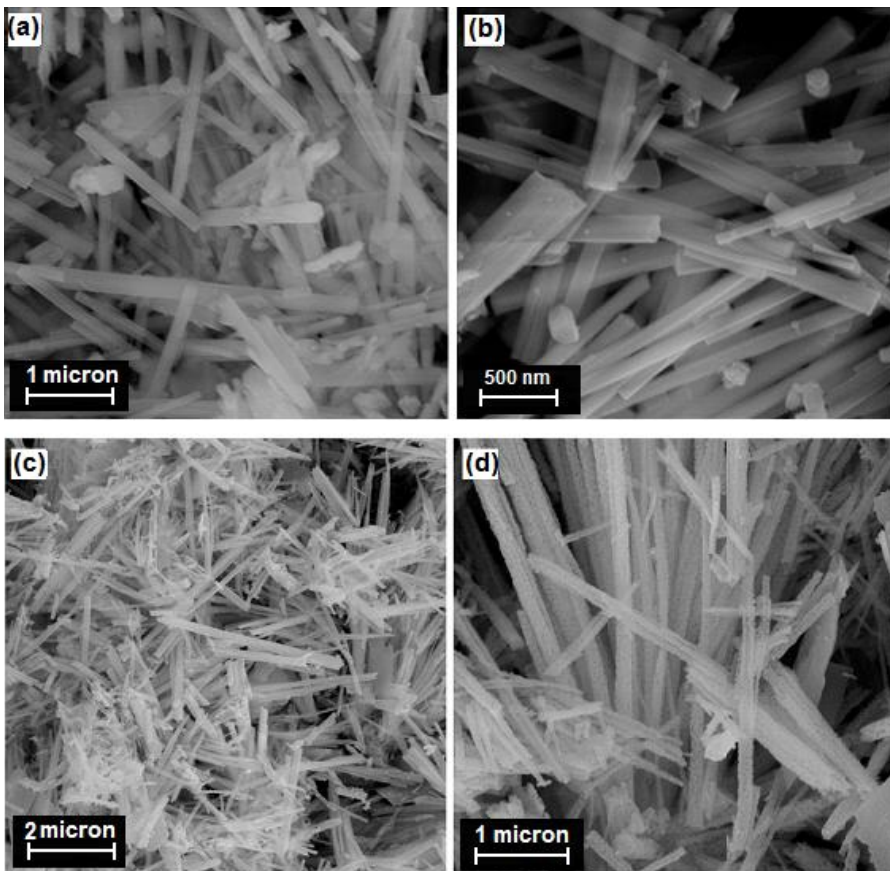

Fig. 3: SEM images of (a) the $CoC_2O_4.2H_2O$ complex and (b) its decomposition product under MWI.

composed of nanoparticles with sizes in the range of 20–30 nm, which is consistent with the above-calculated value by the Scherrer equation. The SAED pattern in Fig. 4(d) shows crystalline nature of Co_3O_4 nanorods. The rings of the SAED pattern can be indexed as (220), (311), (400), (422), (440), (511), (533) and (622) reflections which match well with the reported values of the spinel phase of Co_3O_4.

Fig. 5 *shows* the EDX spectrum of Co_3O_4 nanorods. The spectrum shows that the nanorods are mainly composed of cobalt and oxygen. The presence of Au is due to SEM sample holder. The atomic percentages of Co and O were found to be 43.15% and 56.85%, respectively, which are near to the theoretical values (Co: 42.85 and O: 57.15%) of the Co_3O_4 phase. This observation further confirms that the nanorods are highly pure Co_3O_4.

The Raman spectrum of the Co_3O_4 nanorods is shown in Fig. 6. The Raman spectrum in the range of 400-800 cm^{-1} shows four obvious peaks located at around 465, 590, 608 and 675 cm^{-1}, corresponding to four Raman-active modes (A_{1g}, E_g and $2F_{2g}$) of the Co_3O_4 phase. The Raman shifts are consistent with those of pure crystalline Co_3O_4 [68], indicating that the Co_3O_4 nanorods have a similar crystal structure of the bulk Co_3O_4. This result further confirms the formation of highly pure Co_3O_4 nanorods.

The magnetic property of the Co_3O_4 nanorods was measured using a vibrating sample magnetometer as shown in Fig. 7. The magnetization curve in Fig. 7(a) presents a fine hysteresis loop which is characteristic of weak ferromagnetic behavior although the bulk Co_3O_4 is antiferromagnetic [69]. From Fig. 7(b), the coercive field (H_c) and the remanent magnetization
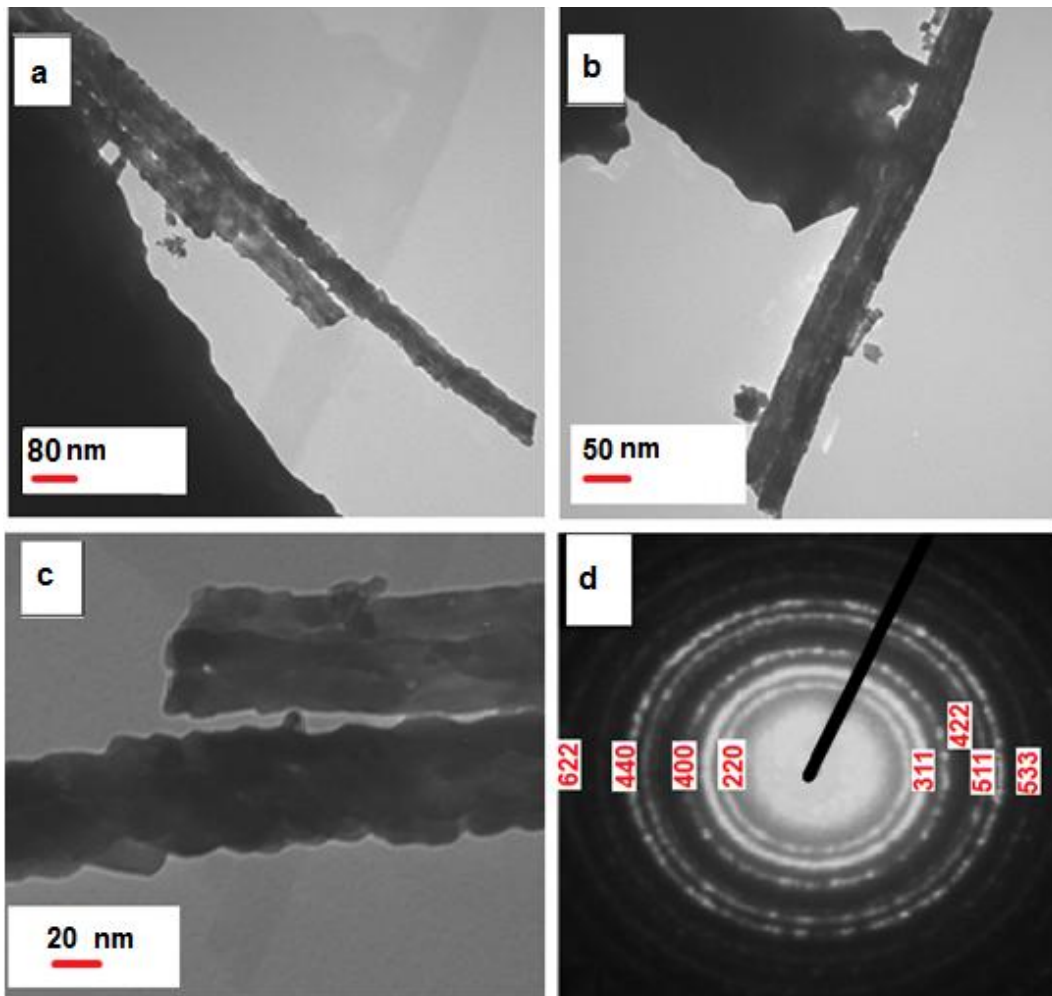

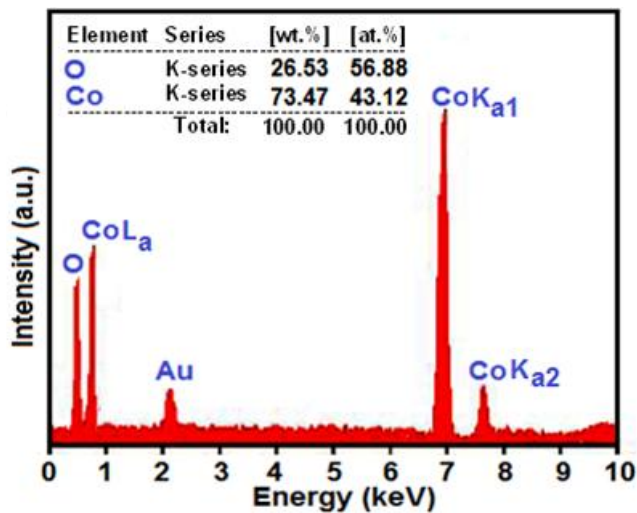Fig. 4: TEM images of the Co_3O_4 nanorods.

S. Bazgir and S. Farhadi
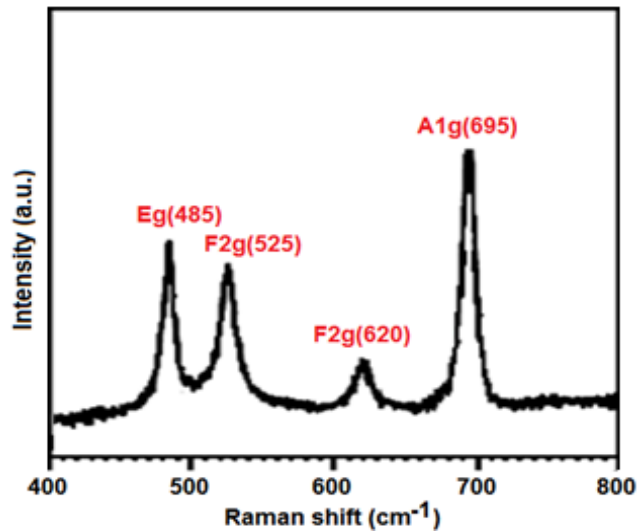

Fig. 5: EDX analysis of the Co₃O₄ nanorods.

Fig. 6: Raman spectrum of the Co₃O₄ nanorods.

(M_r) are estimated to be 15 Oe and 0.001 emu/g, respectively. The low coercive field and remanent magnetization confirm that Co₃O₄ nanorods exhibit a weak ferromagnetic order. The maximum field applied, 8 kOe does not saturate the magnetization and the magnetization at this applied field is 0.275 emu/g. The non-saturation of the magnetization is characteristic of weak ferromagnetic ordering of the spins in the nanostructures. This ferromagnetic behavior of the nanoparticles can be explained as follows: Bulk Co₃O₄ has a normal spinel structure with an antiferromagnetic exchange between ions occupying tetrahedral and octahedral sites [69]. It

has zero net magnetization due to the complete compensation of sublattice magnetizations. Co₃O₄ nanostructures are made of small magnetic domains.

Each magnetic domain is characterized by its own magnetic moment oriented randomly. The total magnetic moment of the nanoparticles is the sum of these magnetic domains coupled by dipolar interactions. Hence, the change from an antiferromagnetic state for bulk Co₃O₄ to a weakly ferromagnetic state for Co₃O₄ nanorods can be ascribed to the uncompensated surface spins and/or finite size effects [70].

290

The optical properties of the Co_3O_4 nanorods were investigated by UV–Vis spectroscopy. Fig. 8 shows the UV–vis optical spectrum of the Co_3O_4 nanorods with two absorption bands in the wavelength ranges of 250–350 and 400–600 nm. The first band can be assigned to the $O^{2-} \rightarrow Co^{2+}$ charge transfer process while the second one related to the $O^{2-} \rightarrow Co^{3+}$ charge transfer [71]. Co_3O_4 is a p-type semiconductor and the absorption band gap (E_g) can be determined by the following equation [30]: $(\alpha h\nu)^2 = K(h\nu - E_g)$ where $h\nu$ is the photon energy (eV), α is the absorption coefficient, K is a constant and E_g is the band gap. The band gap can be estimated by extrapolating the linear region of the plot of $(\alpha h\nu)^2$ versus $h\nu$. As shown in the inset of Fig. 8, two absorption bands give two E_g values at 2.20 and 3.60 eV for the product which are blue-shifted relative to reported values for the bulk sample data (1.77 and 3.37 eV, respectively) [72]. The increase in the band gaps of the Co_3O_4 nanorods can be related to the small size effects of nanoparticles. Owing to the existence of a narrow band gap (E_g = 2.20 eV), Co_3O_4 nanorods are expected to be a visible light photocatalyst with high activity to degrade important pollutants such as organic dyes in wastewater.

Photocatalytic activity of Co_3O_4 nanorods

The photocatalytic activity of the as-prepard Co_3O_4 nanorods was evaluated by the degradation of methylene blue (MB) in aqueous solution as a model of pollutant under visible light irradiation. The concentration changes of MB at 663 nm as a function of irradiation time under different conditions are shown in Fig. 9(a). The concentration changes and percentage of degradation were calculated by C/C_0, where the C represents the concentration of remained dye in solution at the certain irradiation time interval, while the C_0 is the initial concentration of dye solution before irradiation. Curve i in Fig. 9(a) shows that negligible amounts of MB were degraded in the absence of visible-light irradiation and in dark. Curves ii and iii in Fig. 9(a) show that the degradation percentages of MB in the presence of Co_3O_4 nanorods (without H_2O_2) and with H_2O_2 alone (without Co_3O_4 nanorods) after 160 min irradiation are about 10, and 18%, respectively. Curves iv, v, and vi in Fig. 9(a) show that in the presence of both (Co_3O_4 nanorods and H_2O_2 system), the degradation of MB under visible light irradiation increases. Curves iv and iii in Fig. 9(a) show the degradation of MB

with different amounts of catalyst. As can be seen, with increasing Co_3O_4 dosages from 10 to 20 and then to 30 mg, the photocatalytic efficiency of MB degradation was found to be 54, 83 and 100% respectively, in 160 min. The more Co_3O_4 nanorods in the solution provide more active reaction sites for the generation of $^{•}OH$ radicals, increasing the degradation efficiency. The above results confirmed that the visible light irradiation, H_2O_2, and Co_3O_4 nanorods are necessary to achieve fast and complete degradation of the dyes.

The UV-vis spectral changes of MB aqueous solution over Co_3O_4 nanorods (30 mg) photocatalyst are plotted in Fig. 9(b) as a function of irradiation time. It shows that the intensity of characteristic absorption peak of MB at 663 nm decreases gradually as time increases and nearly disappears within 160 min, indicating the complete degradation of MB molecules. Therefore, the photocatalytic experiments show that the as-prepared Co_3O_4 nanorods have a high visible light photocatalytic activity for the degradation of MB organic dye.

The trapping experiments were employed to detect the active species during photocatalytic process. Isopropanol (IPA), Na_2EDTA, and Ag^+ were added into the photocatalytic reaction system as scavengers for $^{•}OH$, e^-_{CB} and h^+_{VB} respectively [73, 74]. As it is illustrated in Fig. 10, we can see that the slight or moderate inhibition of MB degradation was observed in the presence of Ag^+ and Na_2EDTA, indicating that electrons and holes are not the main reactive species in the Co_3O_4 nanorods/H_2O_2 system. However, it can be found that the degradation of MB was greatly decreased when IPA was introduced, indicating that $^{•}OH$ radicals are the significant active species in the photocatalytic reaction.

Based on the above experimental results, a mechanism for the degradation of MB over Co_3O_4 nanorods under visible light irradiation is proposed and illustrated in Fig. 11. Under irradiation with visible light, Co_3O_4 nanorods with E_g = 2.2 eV can absorb the photon energy and produce the electron-hole pairs (Eq. (1)).

The collective photoinduced electrons on the CB of Co_3O_4 nanorods could react with H_2O_2 molecules to generate $^{•}OH$ radicals (Eq. (2)).

Meanwhile, photoinduced holes from valence band (VB) would be immigrated to the surface of Co_3O_4 nanorods and further reacted with the absorbed H_2O molecules or hydroxide ion (OH^-) to form $^{•}OH$ radicals (Eq. (3)).
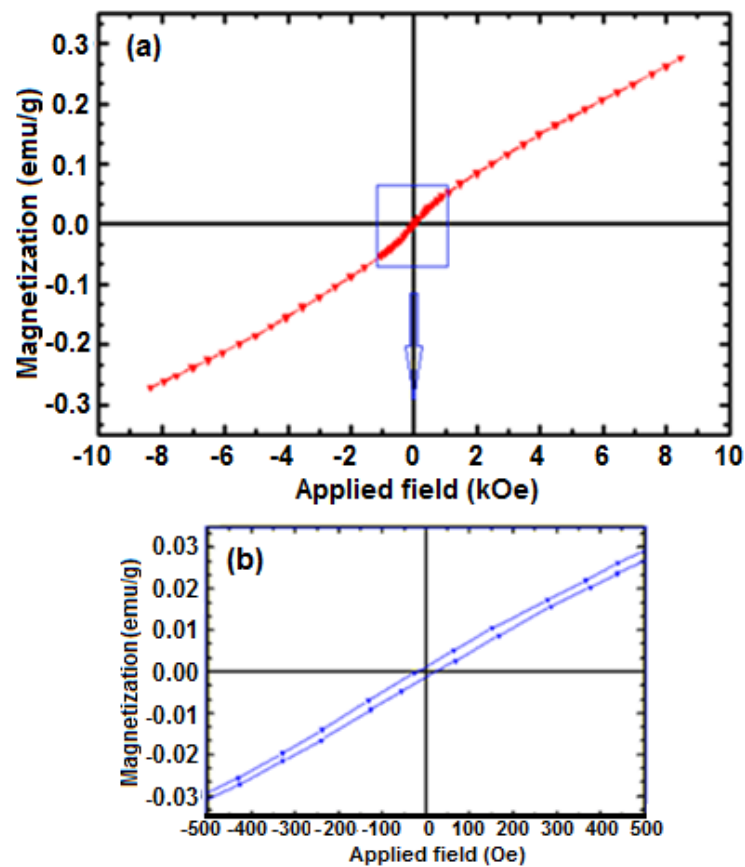
S. Bazgir and S. Farhadi

Fig. 7: (a) The curve of magnetization vs. applied magnetic field for the Co_3O_4 nanorods and (b) Enlarged view of the hysteresis loop in the low-field region.
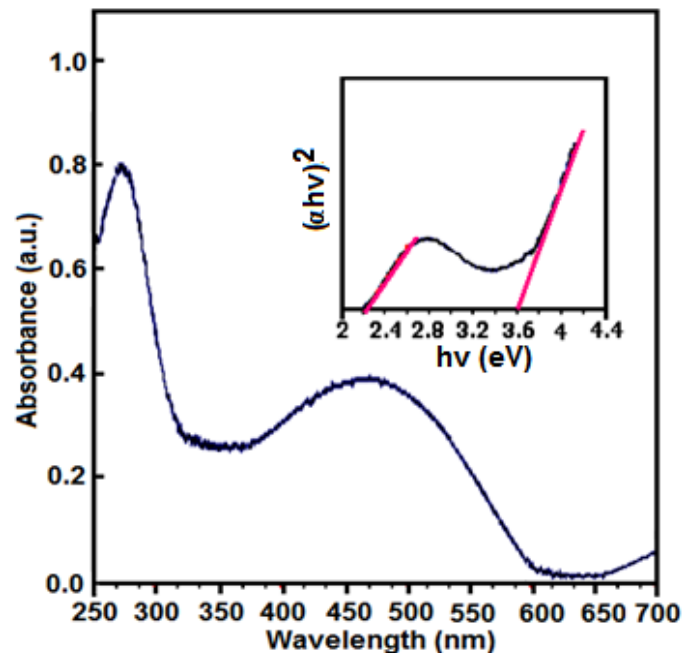

Fig. 8: UV-Vis spectrum and $(\alpha h\nu)^2$-hv curve (inset) of the Co_3O_4 nanorods.
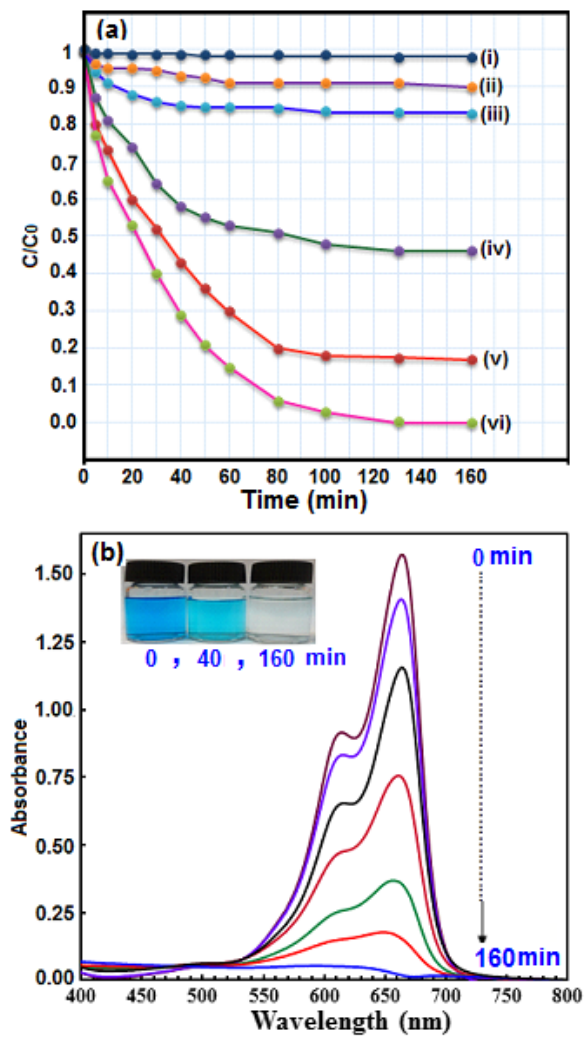
S. Bazgir and S. Farhadi

Fig. 9: (a) Concentration changes of MB as a function of irradiation time under different conditions, and (b) The temporal evolution of absorbance spectrum of MB aqueous solution (50 mL, 25 mg/L) in the presence of Co_3O_4 nanorods (30 mg) and H_2O_2 (30 %, 1 mL) under visible light irradiation at different intervals.
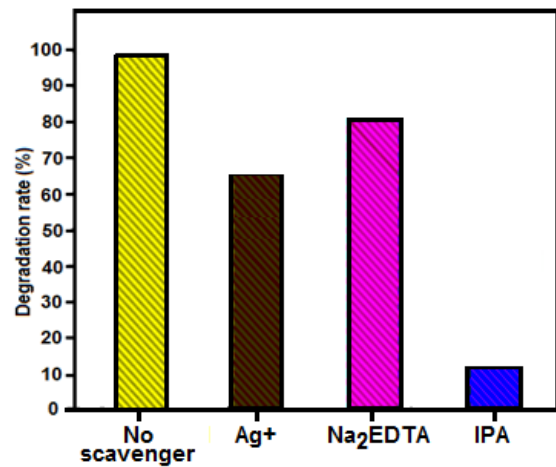

Fig. 10: Effect of various scavengers on the photocatalytic degradation of MB over Co_3O_4 nanorods for 160 min.
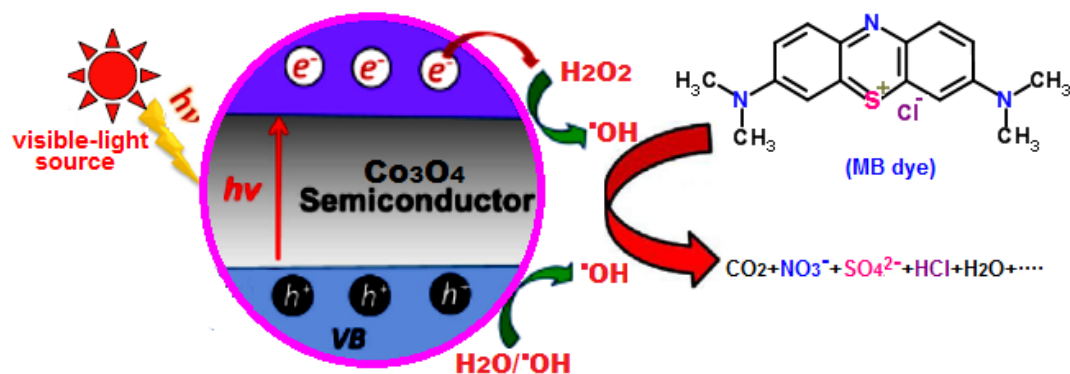
Fig. 11: Schematic illustration of the photocatalytic process of Co_3O_4 nanorods /H_2O_2 system for the degradation of MB in aqueous solution.
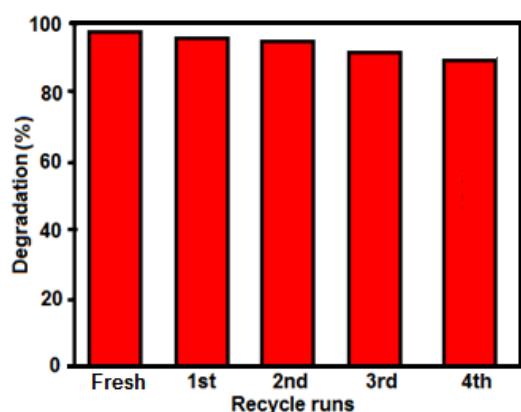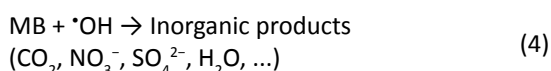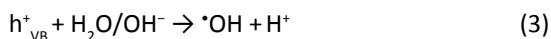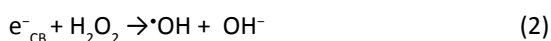

Fig. 12: Recyclability of the Co_3O_4 nanorods in the photodegradation of MB under visible light irradiation.

Fig. 13: (a) XRD pattern, and (b) FT-IR spectrum of the recovered Co_3O_4 nanorods photocatalyst.

The generated active $^{\bullet}$OH radicals effectively react to degrade the dye molecules to CO_2, H_2O or other products (Eq. (4)).

The proposed mechanism of photocatalytic dye degradation using Co_3O_4 nanorods can be described as follows (Fig. 11):

$$Co_3O_4 + \text{visible light} \rightarrow e^-_{CB} + h^+_{VB} \quad (1)$$

$$e^-_{CB} + H_2O_2 \rightarrow {^{\bullet}OH} + OH^- \quad (2)$$

$$h^+_{VB} + H_2O/OH^- \rightarrow {^{\bullet}OH} + H^+ \quad (3)$$

$$MB + {^{\bullet}OH} \rightarrow \text{Inorganic products}$$
$$(CO_2, NO_3^-, SO_4^{2-}, H_2O, ...) \quad (4)$$
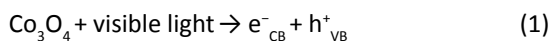
To investigate the recyclability of the Co_3O_4 photocatalyst, the repeated photocatalytic experiments have been done under the same conditions. As shown in Fig. 12, after four consecutive runs of MB degradation, the activity of Co_3O_4 nanorods only exhibited a slight

deactivation. Furthermore, the structural stability of recovered Co_3O_4 photocatalyst was confirmed by XRD and FT-IR after four runs. As shown in Fig. 13(a and b), XRD pattern and FT-IR spectrum of the recovered photocatalyst did not show a change in comparison with those of the fresh catalyst (see Figs. 1(b) and 2(b)). This observation confirms that the structure of the Co_3O_4 nanorods is stable under the reaction conditions and was not affected by the reactants.

CONCLUSIONS

In conclusion, we have developed a simple and green method to synthesize spinel-type Co_3O_4 nanorods with the diameter in the range of 40 to 80 nm via microwave-assisted decomposition of the rod-like $CoC_2O_4 \cdot 2H_2O$ precursor. By this method, Co_3O_4 nanorods with weak ferromagnetic behavior can be obtained rapidly without using a solvent/surfactant and complicated equipment. The optical absorption band gaps of the Co_3O_4 nanorods were estimated to be about 2.20 and 3.60 eV, which show some blue shift in comparison with the bulk sample. This method is simple, low-cost, safe and suitable for the synthesis of high purity Co_3O_4 nanorods for various applications. Photocatalytic measurement demonstrated that the as-synthesized Co_3O_4 nanorods display good degradation efficiency for MB dye.

ACKNOWLEDGEMENTS

CONFLICT OF INTEREST

The authors declare that there is no conflict of interests regarding the publication of this manuscript.

REFERENCES

[1] Klabunde K. J., Richards R. M., (2012), *Nanoscale Materials in Chemistry*. 2nd edn. Wiley, New York.

[2] Mate V. R., Shirai M., Rode C. V., (2013), Heterogeneous Co_3O_4 catalyst for selective oxidation of aqueous veratryl alcohol using molecular oxygen. *Catal. Commun.* 33: 66–69.

[3] Warang T., Patel N., Santini A., Bazzanella N., Kale A., Miotello, A, (2012), Pulsed laser deposition of Co_3O_4 nanoparticles assembled coating: Role of substrate temperature to tailor disordered to crystalline phase and related photocatalytic activity in degradation of methylene blue. *Appl. Catal. A: Gen.* 423–424: 21– 27.

[4] Casas-Cabanas M., Binotto G., Larcher D., Lecup A., Giordani V., Tarascon, J. M., (2009), Defect chemistry and catalytic activity of nanosized. Co_3O_4. *Chem. Mater.* 21: 1939–1947.

[5] Askarinejad A., Bagherzadeh M., Morsali A, (2010), Catalytic performance of Mn_3O_4 and Co_3O_4 nanocrystals prepared by sonochemical method in epoxidation of styrene and cyclooctene. *Appl. Surface Sci.* 256: 6678–6682.

[6] Lou X. W., Deng D., Lee J. Y., Feng J., Archer L. A., (2008), Self-supported formation of needlelike Co_3O_4 nanotubes and their application as lithium-ion battery electrodes. *Adv. Mater.* 20: 258–262.

[7] Chou S. L., Wang J. Z., Liu H. K., Dou S. X., (2008), Electrochemical deposition of porous Co_3O_4 nanostructured thin film for lithium-ion battery. *J. Power. Sources.* 182: 359–364.

[8] Li Y. G., Tan B., Wu Y. Y., (2008), Mesoporous Co_3O_4 nanowire arrays for lithium ion batteries with high capacity and rate capacity. *Nano Lett.* 8: 265-270.

[9] Li W.Y., Xu L. N., Chen J., (2005), Co_3O_4 nanomaterials in lithium-ion batteries and gas sensors. *Adv. Func. Mater.* 15: 851-857.

[10] Sugimoto T., Matijevic E., (1979), Colloidal cobalt hydrous oxides, preparation and properties of monodispersed. Co_3O_4. *J. Inorg. Nucl. Chem.* 41: 165-172.

[11] Makhlouf S. A., (2002), Magnetic properties of Co_3O_4 nanoparticles. *J. Magn. Magn. Mater.* 246: 184–190.

[12] Sun L., Li H., Ren L., Hu C., (2009), Synthesis of Co_3O_4 nanostructures using a solvothermal approach. *Solid State Sci.* 11: 108–112.

[13] Chen Y., Zhang Y., Fu S., (2007), Synthesis and characterization of Co_3O_4 hollow spheres. *Mater. Lett.* 61: 701–705.

[14] Masoomi M. Y., Morsali A., (2012), Applications of metal-organic coordination polymers as precursors for preparation of nano-materials. *Coord. Chem. Rev.* 256: 2921-2943.

[15] Mohandes F., Davar F., Salavati-Niasari M., (2010), Preparation of Co_3O_4 nanoparticles by nonhydrolytic thermolysis of $[Co(Pht)(H_2O)]_n$ polymers. *J. Magn. Magn. Mater.* 322: 872–877.

[16] Kodge A., Kalyane S., Lagashetty A., (2012), Synthesis, characterization and thermal study of poly (methyl methacrylate)-Co_3O_4 nanocomposite film. *Int. J. Nano Dimens.* 3: 53-57.

[17] Thangavelu K., Parameswari K., Kuppusamy K., Haldorai Y., (2011), A simple and facile method to synthesize Co_3O_4 nanoparticles from metal benzoate dihydrazinate complex as a precursor. *Mater. Lett.* 65: 1482–1484.

[18] Salavati-Niasari M., Khansari A., Davar F., (2009), Synthesis and characterization of cobalt oxide nanoparticles by thermal treatment process. *Inorg. Chim. Acta.* 362: 4937–4942.

[19] Farhadi S., Pourzare K., (2012), Simple and low-temperature preparation of Co_3O_4 sphere-like nanoparticles via solid-state thermolysis of the $[Co(NH_3)_6](NO_3)_3$ complex. *Mater. Res. Bull*. 47: 1550–1556.

[20] Farhadi S., K. Pourzare, (2014), Synthesis and characterization of Co_3O_4 nanoplates by simple thermolysis of the $[Co(NH_3)_6]_2(C_2O_4)_3 \cdot 4H_2O$ complex. *Polyhedron.* 67: 104–110.

[21] Farhadi S., Nadri Gh., Javanmard M., (2016), $[Co(NH_3)_5(NO_3)]$ $(NO_3)_2$ as an energetic coordination precursor for the preparation of Co_3O_4 nanoparticles at low temperature. *Int. J. Nano Dimens.* 7: 201-207.

[22] Li L., Chu Y., Liu Y., Song J. L., Wang D., Du X. W., (2008), A facile hydrothermal route to synthesize novel Co_3O_4 nanoplates. *Mater. Lett.* 62: 1507–1510.

[23] Du J., Chai L., Wang G., Li K., Qian Y., (2008), Controlled synthesis of one-dimensional single-crystal Co_3O_4 nanowires. *Aust. J. Chem.* 61: 153–158.

[24] Wang R. M., Liu C. M., Zhang H. Z., Chen C. P., Guo L., Xu H. B., Yang S. H., (2004), Porous nanotubes of Co_3O_4: Synthesis, characterization and magnetic properties. *Appl. Phys. Lett.* 85: 2080–2082.

[25] Li Y., Zhao J., Dan Y., Ma D., Zhao Y., Hou S., Lin H., Wang Z., (2011), Low temperature aqueous synthesis of highly dispersed Co_3O_4 nanocubes and their electrocatalytic activity studies. *Chem. Eng. J.* 166: 428–434.

[26] Sun H., Ahmad M., Zhu J., (2013), Morphology-controlled synthesis of Co_3O_4 porous nanostructures for the application as lithium-ion battery electrode. *Electrochim. Acta.* 89: 199-205.

[27] Ren M., Yuan S., Su L., Zhou Z., (2012), Chrysanthemum-like Co_3O_4 architectures: Hydrothermal synthesis and

lithium storage performances. *Solid State Sci.* 14: 451-455.

[28] Yang L. X., Zhu Y. J., Li L., Zhang L., Tong H., Wang W. W., (2006), A facile hydrothermal route to flower-like cobalt hydroxide and oxide. *Eur. J. Inorg. Chem.* 23: 4787–4792.

[29] Jiu J., Ge Y., Li X., Nie L., (2002), Preparation of Co_3O_4 nanoparticles by a polymer combustion route. *Mater. Lett.* 54: 260–263.

[30] Gu F., Li C., Hu Y., Zhang L., (2007), Synthesis and optical characterization of Co_3O_4 nanocrystals via a facile combustion method. *J. Crys. Growth.* 304: 369–373.

[31] Gardey-Merino M. C., Palermo M., Belda R., Fernández de Rapp M. E., Lascalea G. E., Vázquez P. G., (2012), Combustion synthesis of Co_3O_4 nanoparticles: fuel ratio effect on the physical properties of the resulting powders. *Proced. Mater. Sci.* 1: 588-593.

[32] Ma J., Zhang S., Liu W., Zhao Y., (2010), Facile preparation of Co_3O_4 nanocrystals via a solvothermal process directly from common Co_2O_3 powder. *J. Alloys Compd*. 490: 647–651.

[33] Lester E., Aksomaityte G., Li J., Gomez S., Gonzalez-Gonzalez J., Poliakoff, M., (2012), Controlled continuous hydrothermal synthesis of cobalt oxide (Co_3O_4) nanoparticles. *Prog. Cryst. Growth Charact. Mater.* 58: 3–13.

[34] Baydi M. E., Poillerat G., Rehspringer J. L., Gautier J. L., Koenig J. F., Chartier P., (1994), A sol–gel route for the preparation of Co_3O_4 catalyst for oxygen electrocatalysis in alkaline medium. *J. Solid State Chem.* 109: 281–288.

[35] Kim D. Y., Ju S. H., Koo H. Y., Hong S. K., Kangf Y. C., (2006), Synthesis of nanosized Co_3O_4 particles by spray pyrolysis. *J. Alloys Compd.* 417: 254–258.

[36] Kumar R. V., Diamant Y., Gedanken A., (2000), Sonochemical synthesis and characterization of nanometer-size transition metal oxides from metal acetates. *Chem. Mater.* 12: 2301–2305.

[37] Wang X., Chen X. Y., Gao L. S., Zheng H. G., Zhang Z., Qian, Y. T., (2004), One-dimensional arrays of Co_3O_4 nanoparticles: Synthesis, characterization and optical and electrochemical properties. *J. Phys. Chem. B.* 108: 16401–16404.

[38] Fan S., Liu X., Li Y., Yan E., Wang C., Liu J., Zhang Y., (2013), Non-aqueous synthesis of crystalline Co_3O_4 nanoparticles for lithium-ion batteries. *Mater. Lett.* 91: 291–293.

[39] Jiang J., Li L., (2007), Synthesis of sphere-like Co_3O_4 nanocrystals via a simple polyol route. *Mater. Lett.* 61: 4894–4896.

[40] Zou D., Xu C, Luo H., Wang L., Ying T., (2008), Synthesis of Co_3O_4 nanoparticles via an ionic liquid-assisted methodology at room temperature. *Mater. Lett.* 62: 1976–1978.

[41.] Zhou K., Liu J., Wen P., Hu Y., Gui Z., (2015), Morphology-controlled synthesis of Co_3O_4 by one step template-free hydrothermal method. *Mater. Res. Bull.* 67: 87–93.

[42] Zhu Y. J., Chen F., (2014), Microwave-assisted preparation of inorganic nanostructures in liquid phase. *Chem. Rev.* 114: 6462–6555.

[43] Kitchen H. J., Vallance S. R., Kennedy J. L., Tapia-Ruiz N., Carassiti L., Harrison A., Whittaker A. G., Drysdale T. D., Kingman S. W., Gregory D. H., (2014), Modern microwave methods in solid-state inorganic materials chemistry: From fundamentals to manufacturing. *Chem. Rev.* 114: 1170–1206.

[44] Assi N., Sharif A. M., Naeini, Q. M., (2014), Synthesis, characterization and investigation photocatalytic degradation of Nitro Phenol with nano ZnO and ZrO_2. *Int. J. Nano Dimens.* 5: 387-391.

[45] Assi N., Sharif A. M., Bakhtiari H., Naeini Q. M., (2014), Photocatalytic property of ZnO and Mn-ZnO nanoparticles in removal of Cibacet Turquoise blue G from aquatic

solution. *Int. J. Nano Dimens.* 5: 145-154.

[46] Majedi A., Davar F., Abbasi A. R., (2016), Metal-organic framework materials as nano photocatalyst. *Int. J. Nano Dimens.* 6: 1-14.

[47] Khodadadeh F., Aberoomand-Azar P., Tehrani M. S., Assi N., (2016), Photocatalytic degradation of, 2, 4, 6-Trichlorophenol with CdS nanoparticles synthesized by a microwave-assisted sol-gel method. *Int. J. Nano Dimens.* 7: 263-269.

[48] Nakata K., Fujishima A., (2012), TiO_2 photocatalysis: Design and applications. *J. Photochem. Photobiol. C: Photochem. Rev.* 13: 169-189.

[49] Janitabar Darzi S., Mahjoub A. R., Bayat A., (2016), Synthesis and characterization of visible light active S-doped TiO_2 nanophotocatalyst. *Int. J. Nano Dimens.* 7: 33-40.

[50] Abbasi A., Jahanbin-Sardroodi J., (2016), A theoretical study on the adsorption behaviors of ammonia molecule on N-doped TiO_2 anatase nanoparticles: Applications to gas sensor devices. *Int. J. Nano Dimens.* 7: 349-359.

[51] Rastkar -Ebrahimzadeh A., Abbasi M., Jahanbin Sardroodi J., Afshari S., (2015), Density functional theory study of the adsorption of NO_2 molecule on nitrogen-doped TiO_2 anatase nanoparticles. *Int. J. Nano Dimens.* 6: 11-17.

[52] Zakeri S. M. E., Asghari M., Feilizadeh M. Vosoughi M., (2014), A visible light driven doped TiO_2 nanophotocatalyst: Preparation and characterization. *Int. J. Nano Dimens.* 5: 329-335.

[53] Khojasteh, H., Salavati-Niasari, M., Mazhari, M.-P., Hamadanian, M., (2016), Preparation and characterization of $Fe_3O_4@SiO_2@TiO_2@Pd$ and $Fe_3O_4@SiO_2@TiO_2@Pd–Ag$ nanocomposites and their utilization in enhanced degradation systems and rapid magnetic separation. *RSC Adv.* 6: 78043-78052.

[54] Safajou H., Khojasteh H., Salavati-Niasari M., Mortazavi-Derazkola S., (2017), Enhanced photocatalytic degradation of dyes over graphene/Pd/TiO_2 nanocomposites: TiO_2 nanowires versus TiO_2 nanoparticles. *J. Coll. Interf. Sci.* 498: 423-432.

[55] Aghabeygi Sh., Zare-Dehnavi M., (2015), Sonosynthesis and characterization of ZrO_2/ZnO nanocomposite, composition effect on enhancing of photocatalytic properties. *Int. J. Nano Dimens.* 6: 297-304.

[56] Hoseini L., Bagheri-Ghomi A., (2016), Photocatalytic degradaton of Sulfathiazole using nanosized CdO in aqueous solution. *Int. J. Nano Dimens.* 8: 159-163.

[57] Azar-Bagheri Gh., Ashayeri V., Mahanpoor K., (2013), Photocatalytic efficiency of $CuFe_2O_4$ for photodegradation of acid red 206. *Int. J. Nano Dimens.* 4: 111-115.

[58] Assi N., Aberoomand-Azar P., Tehrani M. S., Husain S. W., Darwish M., Pourmand S., (2017), Synthesis of ZnO-nanoparticles by microwave assisted sol-gel method and its role in photocatalytic degradation of food dye Tartrazine (Acid Yellow 23). *Int. J. Nano Dimens.* 8: 241-249.

[59] Wang Y., Zhou L., Duan X., Sun H., Tin E. L., Jin W., Wang S., (2015), Photochemical degradation of phenol solutions on Co_3O_4 nanorods with sulfate radicals. *Catal.Today.* 25: 576-584.

[60] Qiu X. P., Yu J. S., Xu H. M., Chen W. X., Hu W., Chen G. L., (2016), Interfacial effects of the Cu_2O nano-dots decorated Co_3O_4 nanorods array and its photocatalytic activity for cleaving organic molecules. *Appl. Surf. Sci.* 382: 249-259.

[61] Lai, T.-L., Lai, Y.-L., Lee, C.-C., Shu, Y.-Y., Wang, C.-B., (2008), Microwave-assisted rapid fabrication of Co_3O_4 nanorods and application to the degradation of phenol. *Catal. Today.* 131: 105-110.

[62] Gasparotto A., Barreca D, Bekermann D., Devi A., Fischer R. A., Fornasiero P., Gombac V., Lebedev O. I., Maccato C., Montini T., Tendeloo G. V., Tondello E., (2011), F-Doped Co_3O_4 photocatalysts for sustainable H_2 generation from water/ethanol. *J. Am. Chem. Soc.* 133: 19362–19365.

[63] Salavati-Niasari M., Mir N., Davar F., (2009), Synthesis and characterization of Co_3O_4 nanorods by thermal decomposition of cobalt oxalate. *J. Phys. Chem. Solids.* 70: 847–852.

[64] Nakamoto K., (2009), Infrared and Raman spectra of inorganic and coordination compounds, Part B: Applications in coordination, organometallic and bioinorganic chemistry, 6th edn. *Wiley,* New York.

[65] Ai L. H., Jiang J., (2009), Rapid synthesis of nanocrystalline Co_3O_4 by a microwave-assisted combustion method. *Powder Tech.* 195: 11–14.

[66] Bhatt A. S., Bhat D. K., Tai C. W., Santosh M. S., (2011), Microwave-assisted synthesis and magnetic studies of cobalt oxide nanoparticles. *Mater. Chem. Phys.* 125: 347–350.

[67] Klug H. P., Alexander L. E., (1964), X-ray Diffraction Procedures, 2nd edn. *Wiley*, New York.

[68] Nethravathi C., Sen S., Ravishankar N., Rajamathi M., Pietzonka C., Harbrecht B., (2005), Ferrimagnetic nanogranular Co_3O_4 through solvothermal decomposition of colloidally dispersed monolayers of α-cobalt hydroxide. *J. Phys. Chem. B.* 109: 11468 –11472.

[69] Ichiyanagi Y., Kimishima Y., Yamada S., (2004), Magnetic study on Co_3O_4 nanoparticles. *J. Magn. Magn. Mater.* 272–276: e1245–e1246.

[70] Ozkaya T., Baykal A., Toprak M. S., Koseoglu Y, Durmus Z., (2009), Reflux synthesis of Co_3O_4 nanoparticles and its magnetic characterization. *J. Magn. Magn. Mater.* 321: 2145–2149.

[71] He T., Chen D. R., Jiao X. L., Wang Y. L., Duan Y. Z., (2005), Solubility-controlled synthesis of high-quality Co_3O_4 nanocrystals. *Chem. Mater.* 17: 4023–4030.

[72] Gulino A., Dapporto P., Rossi P., Fragala I., (2003), A novel self-liquid MOCVD precursor for Co_3O_4 thin films. *Chem. Mater.* 15: 3748–3752.

[73] Yu K., Yang S., Liu C., Chen H., Li H., Sun C., Boyd S. A., (2012), TiO_2-assisted photodegradation of dyes. 9. Photooxidation of a squarylium cyanine dye in aqueous dispersions under visible light irradiation. *Environ. Sci.Technol.* 46: 7318–7326.

[74] Zhang H., Lv X., Li Y., Wang Y., Li J., (2010), P25-Graphene composite as a high performance photocatalyst. *ACS Nano.* 4: 380–386.